Received: 22 February 2023 | Revised: 19 April 2023 | Accepted: 26 April 2023

DOI: 10.1002/cjce.24967

RESEARCH ARTICLE

THE CANADIAN JOURNAL OF CHEMICAL ENGINEERING

Optimizing the synthesis of Ag/γ-Al_2O_3 for selective reduction of NOx with C_3H_6: Experiments and modelling

Shivaraj Kumar Kummari[1,2] | **Neha Yedala**[1] | **Parasuraman Selvam**[2,3,4] | **Niket S. Kaisare**[1,2] | **Preeti Aghalayam**[1,2]

[1]Department of Chemical Engineering, Indian Institute of Technology-Madras, Chennai, India

[2]National Centre for Catalysis Research, Indian Institute of Technology-Madras, Chennai, India

[3]Department of Chemistry, Indian Institute of Technology-Madras, Chennai, India

[4]School of Chemical Engineering and Analytical Science, The University of Manchester, Manchester, UK

Correspondence
Preeti Aghalayam, Department of Chemical Engineering, Indian Institute of Technology-Madras, Chennai, 600036, India.
Email: preeti@iitm.ac.in

Funding information
Department of Science and Technology, Ministry of Science and Technology, India, Grant/Award Number: Ucchatar Avishkar Yojana (UAY)

Abstract

Ag/γ-Al_2O_3 is an effective catalyst for the selective reduction of NOx (SCR) using propylene as a reducing agent. The catalyst performance is greatly influenced by the synthesis procedure. Various methods for synthesis of Ag/γ-Al_2O_3 are analyzed, and their performance is examined via packed bed reactor experiments in this work. An optimal one-pot synthesis method, single-step sol–gel (SSG) synthesis, is explored systematically. The SSG-synthesized catalyst shows better performance than those prepared via wet impregnation. The influence of synthesis conditions, specifically pH, on the textural and morphological properties of the SSG-synthesized Ag/γ-Al_2O_3, and therefore the activity for hydrocarbon-based SCR in a packed-bed reactor, are analyzed using experiments and simulations. The optimized catalyst demonstrates excellent performance (90% NOx conversion) for NOx reduction under nominal operating conditions with a wide activity temperature window (300–600°C). The catalyst shows good time-on-stream performance and is effective at higher inlet oxygen concentrations and space velocities. A global kinetic model, which uses synthesis-pH-dependent parameters, is proposed, and its ability to predict the activities of these catalysts is validated.

KEYWORDS

Ag/γ-Al_2O_3 catalyst, Nitrogen oxides (NOx), *p*H-controlled synthesis, Selective catalytic reduction (SCR), Single-step sol–gel method

1 | INTRODUCTION

Nitrogen oxide (NOx) emissions from stationary or automotive sources are environmentally damaging as they contribute to the formation of acid rain, photochemical smog, and depletion of tropospheric ozone.[1] In addition to NOx and other pollutants, the exhaust from lean-burn gasoline and diesel engines contains an excess amount of oxygen.[2] Under net-oxidizing conditions, the conventional three-way catalyst favours oxidation reactions rather than the selective reduction of NOx.[2,3] Selective catalytic reduction (SCR) of NOx remains a major challenge in environmental catalysis in these oxygen-rich exhaust conditions.[4] The potential for using hydrocarbons (HCs) as reducing agents has generated interest in HC-SCR. Since NOx emissions are the highest at cold-start conditions, low-temperature light-off of HC-SCR as well as sustained activity at high temperatures, are vital goals.[5–8]

Although several catalysts have been tested for HC-SCR to date, no catalyst seems to be suitable for NOx reduction in lean-burn exhaust conditions. Among various catalysts investigated, silver-based catalysts have shown higher activity at relatively low temperatures,[9,10]

even in the presence of SOx and water vapour.[11,12] In contrast, metal ion-exchanged zeolite catalysts, although used in ammonia-SCR, suffer from low activity for HC-SCR, are inactive at higher temperatures, and have poor hydrothermal resistance.[13–16] Platinum group metal catalysts were also investigated for HC-SCR under lean-burn conditions[17]; however, the formation of N_2O and a narrow temperature region for NO reduction[18,19] were identified as key disadvantages. Experimental and kinetic modelling studies have shown the formation of N_2O over Pt/γ-Al_2O_3 catalysts at low temperatures[20,21] and poisoning of the catalyst surface with oxygen either as chemisorbed O or as Pt oxides owing to the highly oxidizing nature of NO_2.[22] The role of support, such as γ-Al_2O_3, SiO_2,[23–25] as well as ZrO_2, CeO_2, WO_3, TiO_2, and MgO,[25–27] has been investigated. Among all the tested catalysts, γ-Al_2O_3 is the preferred support due to its resistance to hydrothermal conditions and tolerance to the presence of SOx and water vapour in the feed stream. As a result, it is an effective support for Ag—supported catalysts used for the selective reduction of NOx.[24–28] Consequently, Ag supported on γ-Al_2O_3 is chosen in this work based on its higher activity and hydrothermal stability.

The preparation method of Ag-based catalysts affects their structural and textural properties and hence the catalytic performance.[4] Co-precipitation, sol–gel, and impregnation are common methods to prepare Ag/γ-Al_2O_3 catalysts. The Ag/γ-Al_2O_3 catalysts prepared by co-precipitation[4] and precipitation from inverse microemulsions[29] showed lower activity, with significant NOx conversion occurring only at higher temperatures. Several researchers[1,2,4,30–33] used the impregnation method to prepare the Ag/γ-Al_2O_3 catalysts with an aqueous solution of $AgNO_3$ on commercial Al_2O_3 supports. Angelidis and Kruse[12] reported that using silver lactate (instead of $AgNO_3$) during the impregnation process led to a homogeneous distribution of Ag on the Al_2O_3 support and hence a higher de-NOx activity. The Ag/γ-Al_2O_3 catalysts synthesized by the sol–gel method[4,34] performed better than those prepared by co-precipitation and impregnation. The Ag/γ-Al_2O_3 catalysts have been prepared using sol–gel co-gelation[35] and precipitation-gelation[36]; though these catalysts achieved higher NOx conversions, the activity temperature window reported was narrow and not satisfactory.[4,32–34] The Ag/Al_2O_3 catalysts, while promising, have higher light-off temperatures and a narrow range of temperatures at which they are sufficiently active for SCR. The role of synthesis conditions on activity is poorly understood.

Though the synthesis conditions affect the morphology and activity of Ag/Al_2O_3 catalysts, these conditions are not optimized, and their role is not well understood. In this work, Ag/γ-Al_2O_3 catalysts are prepared by a single-step sol–gel (SSG) method and compared with wet impregnation of Ag on both commercial and in-house synthesized γ-Al_2O_3. The SSG method is optimized by preparing the catalysts at different hydrolysis pH using nitric acid as a pH controller during the synthesis. The role of the hydrolysis pH in improving the textural and structural properties of the catalyst—crystallinity of γ-Al_2O_3 phase, surface area and pore geometry, as well as the morological properties such as active metal nanoparticles size and dispersion over the support—is investigated. The role of pH on catalyst activity for HC-SCR is explored, and the synthesis procedure is optimized. A reaction kinetic model that predicts the activity of these catalysts prepared at various values of hydrolysis pH is also proposed and validated.

2 | EXPERIMENTAL SECTION

2.1 | Starting materials

The chemicals of analytical grade were used without further purification. The chemicals, aluminium isopropoxide (AIP; > 98%) and silver nitrate ($AgNO_3$; > 99%) were obtained from Sigma–Aldrich, nitric acid (HNO_3; 69%) from Merck, and commercial γ-alumina (γ-Al_2O_3) from SASOL. The calibration grade gases, namely, propylene (3000 ppm C_3H_6, balance N_2), nitric oxide (3000 ppm NO, balance N_2), oxygen (21 vol.% O_2, balance N_2), and nitrogen (N_2, >99.99% high purity), were purchased from Sri Karumari Amman Gas Agency, Indo Gas and Rana Industrial Gases and Products from Chennai, India and used without further purification.

2.2 | Catalyst preparation

2.2.1 | Wet-impregnation (WI) method

The γ-alumina supported silver (Ag/γ-Al_2O_3) catalysts were prepared by the WI method. A calculated amount of aqueous $AgNO_3$ was added in a drop-wise manner to the commercial γ-Al_2O_3(SASOL) support while stirring constantly. Thereafter, it was dried at 110°C for 1–2 days, followed by calcination in a tubular furnace at 600°C for 6 h at 1°C/min under airflow conditions. For ease of discussion, this catalyst is referred to as Ag/γ-Al_2O_3(SASOL).

For comparison, γ-Al_2O_3 was prepared by the sol–gel technique at a pH of 6.0, referred to hereafter as γ-Al_2O_3 (SG). Subsequently, 5% Ag was impregnated as before, and the resulting catalyst is referred to hereafter as Ag/γ-Al_2O_3(WI); see Table 1.

TABLE 1 Preparation and characterization details of various γ-Al_2O_3 and Ag/γ-Al_2O_3 catalyst samples.

Catalyst	Preparation method	pH	Ag loading (wt.%)	Surface area (m^2/g)	Pore volume (cm^3/g)	Pore size (nm)
γ-Al_2O_3 (SASOL)	-	-	-	180	0.34	5.9
γ-Al_2O_3 (SG)	Sol–Gel	6.0	-	200	0.22	4.3
Ag/γ-Al_2O_3 (SASOL)	Wet impregnation	5.7	5	161	0.32	6.6
Ag/γ-Al_2O_3 (WI)	Wet impregnation	5.7	5	174	0.32	6.2
Ag/γ-Al_2O_3 (4.0)	Single-step sol–gel	4.0	5	56	0.08	4.2
Ag/γ-Al_2O_3 (4.7)	SSG	4.7	5	109	0.10	3.0
Ag/γ-Al_2O_3 (5.0)	SSG	5.0	5	132	0.14	3.6
Ag/γ-Al_2O_3 (5.5)	SSG	5.5	5	170	0.22	4.1
Ag/γ-Al_2O_3 (5.7)	SSG	5.7	5	190	0.25	4.8
Ag/γ-Al_2O_3 (6.0)	SSG	6.0	5	207	0.27	5.0
Ag/γ-Al_2O_3 (5.7)	SSG	5.7	3	165	0.23	4.5
	SSG	5.7	5	190	0.25	4.8
	SSG	5.7	7	178	0.25	4.5

Abbreviations: SSG, single-step sol–gel; WI, wet-impregnation.

2.2.2 | Single-step sol–gel (SSG) method

The Ag/γ-Al_2O_3 catalysts were prepared by SSG method using AIP and silver nitrate ($AgNO_3$) as alumina and silver precursors, respectively. Since the pH of the synthesis medium affects the hydrolysis and condensation processes, nitric acid (69%) was added in various amounts to the stirring solution, and after that, the pH of the stirring solution was measured. Accordingly, the catalysts were synthesized as follows: At first, 10 g of AIP was dissolved in 100 mL of milli-pore water. Nitric acid (69%) was then added in various amounts to the stirring solution and the pH of the synthesis medium was measured. Next, the calculated concentrations of aqueous $AgNO_3$ were added to the stirring solution to get 3–7 wt.% Ag loading. The final values of pH were recorded just before the completion of the reaction synthesis and reported here. The resulting solution was stirred for 24 h. After completion of the gel formation, the sample was dried in a hot air oven at 110°C for 24 h, followed by calcination in a tubular furnace at 600°C for 6 h, at 1°C/min under airflow conditions. The catalysts prepared using the SSG method is referred to hereafter as the Ag/γ-Al_2O_3(x), where x in the parenthesis represents the hydrolysis pH value.

2.3 | Characterization

Powder X-ray diffraction (XRD) measurements were recorded on a Bruker D8 Advance XRD with Cu Kα ($\lambda = 1.5418$ A°) radiation source operating at 40 kV and 30 mA. Nitrogen-physisorption isotherms were obtained in Micromeritics ASAP 2020 surface area analyzer at liquid nitrogen temperature 77 K, in which the catalysts were degassed at 250°C for 12 h before measurements. The specific surface areas (S_{BET}) of the samples were calculated using the Brunauer–Emmett–Teller (BET) method, whereas pore size distribution (D_{BJH}) curves were obtained from Barrett–Joyner–Halenda (BJH) method. The surface morphology and composition of the deposited material were studied using a QUANTA 200-FEI SEM instrument equipped with a METEK energy dispersive X-ray analysis (EDX) system. The sample in powdered form was spread on the carbon tape (adhesive tape, normally used in scanning electron microscopy (SEM) measurements for conduction purposes) and mounted on the SEM sample holder, and imaged. High-resolution transmission electron microscopy (HR-TEM) images were obtained from a JEOL, JEM-2100 Plus transmission electron microscope operated at 200 kV. The powder samples were added to the carbon-coated Cu-grids using the drop-casting method.

2.4 | Reactor details

A packed bed reactor (PBR) connected to an on-line gas analyzer was used to measure the HC-SCR activity, and high-purity N_2 gas was used for purging. The high-purity synthetic gases, namely, propylene (3000 ppm C_3H_6, balance N_2), nitric oxide (3000 ppm NO, balance N_2), and oxygen (21 vol.% O_2, balance N_2) were metered through

mass flow controllers (Bronkhorst High-Tech BV) and mixed to obtain the desired inlet concentrations. The PBR consists of a quartz reactor tube with an 8 mm ID, 12 mm OD, and 1000 mm length placed inside a vertical down-flow furnace (Ants Ceramics Pvt. Ltd.). Cylindrical quartz beads (2 × 4 mm) were used as an inert packing material to ensure uniform flow. The catalyst powders were pelletized, made into small (<2 mm) particles and loaded into the quartz tube reactor and held in place with quartz wool, while the top and bottom of the catalyst bed were packed with the packing material. A *k*-type thermocouple (REOTEMP Instrument Corporation) was used to measure the temperature at the surface of the quartz tube reactor in the furnace. The temperature was controlled within ±1°C using a proportional-integral-derivative controller (PID) temperature controller (Ants-1100PC; Ants Ceramics Pvt. Ltd.). The outlet was connected on-line to a non-dispersive infra-red (NDIR) multi-component gas analyzer (HORIBA—Model VA-3000) to measure NO and NOx ($NO + NO_2$) concentrations in the product gas mixture.

2.5 | Reaction studies

The catalytic measurements were performed in the PBR with 980 ppm NO, 1050 ppm C_3H_6, and 7 vol.% of oxygen for all the prepared catalysts. The feed stream gases with different NO:C_3H_6 ratios from 1:1 to 1:2.2, and oxygen concentration from 3.4 to 12.0 vol.% were used to study the effect of inlet composition. The activity of the catalyst for NOx reduction was studied in the temperature range of 200 to 600°C at ambient pressure, and at various gas hourly space velocities by changing the catalyst volume at different flow rates. The reactor was raised to a temperature of 200°C at a ramping rate of 2°C/min and held at this temperature for an hour while being purged with high-purity N_2. Subsequently, the temperature was raised in steps of 50°C with a ramp rate of 5°C/min and the reaction was carried out by passing the reactant gas mixture. The reactor was held at each temperature for 30 min to reach a steady state before recording the outlet concentration.

3 | RESULTS AND DISCUSSIONS

3.1 | Catalyst characterization

pH and/or the concentrations of acid or base in the sol during the sol–gel transition have a profound influence on the formation of gel structures.[37] The effect of synthesis conditions on the structural, textural, and morphological properties of Ag/γ-Al_2O_3 is discussed below.

3.1.1 | Structural properties

Figure 1 depicts the powder XRD patterns of dried samples of γ-AlO(OH) and Ag/γ-AlO(OH) (alumina precursors after drying at 110°C) prior to calcination as well as the calcined γ-Al_2O_3 and Ag/γ-Al_2O_3 prepared at different pH conditions. In-house synthesized boehmite (γ-AlO(OH)) calcined at 300°C is added for reference in Figure 1A to identify the presence of pseudo-boehmite phase in the dried catalyst samples. The alumina precursors (Figure 1A) exhibit a typical boehmite structure, while the characteristic γ-alumina structure can be seen in Figure 1B. It is reported that at lower pH values, the bayerite phase is commonly observed along with the boehmite phase.[38,39] The bayerite phase is marked with the reverse triangle symbols (▽) and the reference for the boehmite phase and the diffraction planes are indicated in Figure 1A. It shows the formation of bayerite along with the amorphous nature of the pseudo-boehmite phase, at low pH values. An increase in pH enhances the crystallinity of the pseudo-boehmite phase along with a diminishing of the bayerite phase. Further, the basic gel shows a network of boehmite particles interconnected with one another, while the acidic gel displays aggregates[35,36]; these results are in good agreement with high resolution-scanning electron microscopy (HR-SEM) (discussed in Section 3.1.3). Figure 1B shows the XRD patterns of the calcined γ-Al_2O_3 and supported 5%Ag/γ-Al_2O_3 catalysts. The diffraction patterns correspond to typical γ-Al_2O_3 structures.[4,26] The Ag nanoparticles are smaller in size and finely dispersed on the support (this is in good agreement with HR-TEM data discussed in Section 3.1.3). The characteristic reflections overlap with γ-Al_2O_3 and therefore the reflections corresponding to elemental Ag cannot be seen clearly.[24,29]

3.1.2 | Textural characteristics

The N_2-physisorption isotherms with pore size distributions are shown in Figure 2. The samples exhibit typical type-IV isotherms, which indicates that the materials are mesoporous in nature[40] with the hysteresis loops of H1- and H2-types. However, as can be seen from Figure 2, the shape of the hysteresis loops of the samples prepared at low pH and calcined show lower crystallinity (Figure 1B) than the samples prepared at higher pH. At lower pH values, samples exhibit H2-type hysteresis loops (ink-bottle type pore geometry). An increase in pH values beyond pH = 5 leads to type-H1 hysteresis, indicating channel-type pore geometry.[39,41,42] The specific surface area, pore volume, and pore sizes of the prepared catalysts are given in Table 1. The specific surface area for

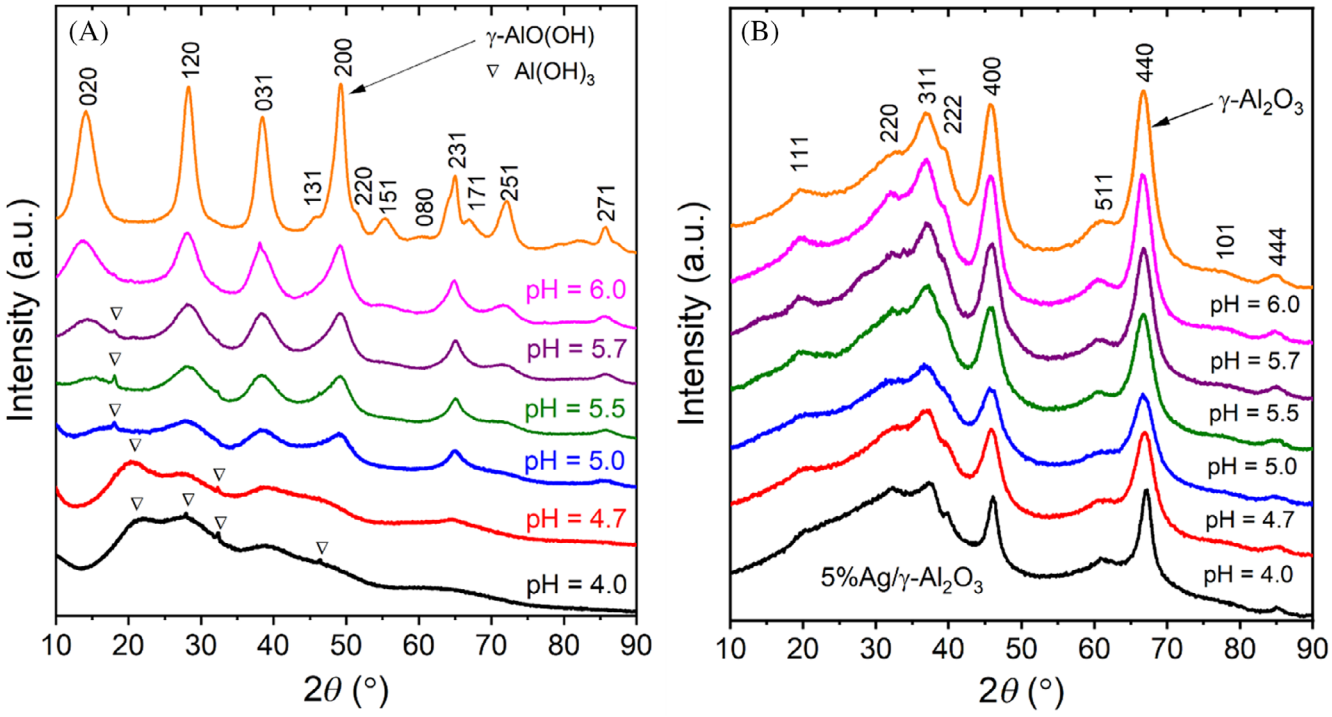

FIGURE 1 Powder X-ray diffraction patterns of dried samples (A) and calcined samples (B) prepared at different pH conditions.

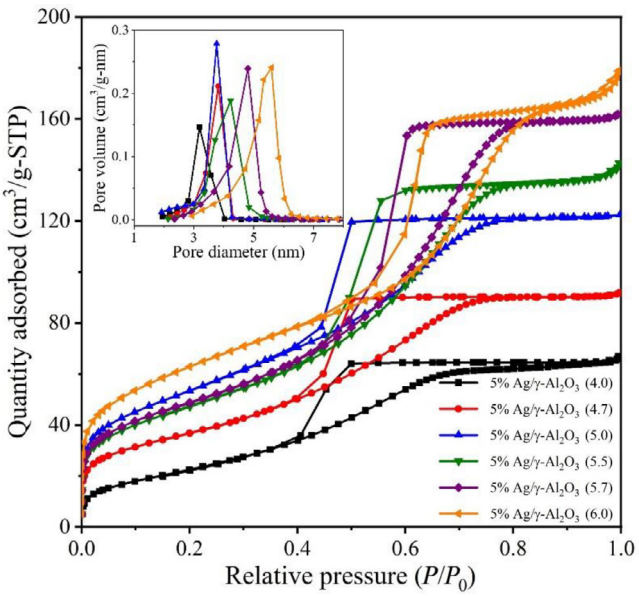

FIGURE 2 Textural properties of the 5% Ag/γ-Al_2O_3 catalysts synthesized using single-step sol–gel method, N_2-physisorption isotherms with pore size distribution. STP, standard temperature and pressure.

the sol–gel prepared γ-Al_2O_3 is 200 m^2g^{-1} while for the commercial γ-Al_2O_3 is 180 m^2g^{-1}. As shown in Table 1, the surface area of the Ag/γ-Al_2O_3 catalysts rises as the pH of the synthesis medium is increased. The specific surface area is increased from 56 m^2g^{-1} for pH = 4.0 to 207 m^2g^{-1} for pH = 6.0; likewise, the pore volume also increased from 0.08 to 0.27 cm^3/g. Furthermore, at lower pH (<5), the pore geometry indicates the ink-bottle type with pore-blocking, whereas with an increase in pH, the pore geometry changed to open mouth ink-bottle type pores, and at higher pH (>5.5), the pores present channel type geometry.

3.1.3 | Morphological properties

Figure 3 depicts the HR-SEM images of various Ag/γ-Al_2O_3 catalysts. At lower pH, the catalysts display aggregated dense large particles; at higher pH, particle size is reduced considerably. In the case of the former, the particles are seen to aggregate just after the addition of nitric acid and bring about a rapid increase of viscosity resulting in the formation of aggregated dense particles. This is because at lower pH, the hydrolysis process is faster and the network formation in the gel process is poorer, and therefore the formation of random dense particles, and the flocculation of particles is promoted by the shielding effect of excess electrolyte (nitric acid in this case).[43] At higher pH, with the addition of very small amounts of nitric acid, a colloidal suspension with constant low viscosity is formed. That is, there is a phase transformation of boehmite particles from the randomly aggregated state to an ordered state of the smaller

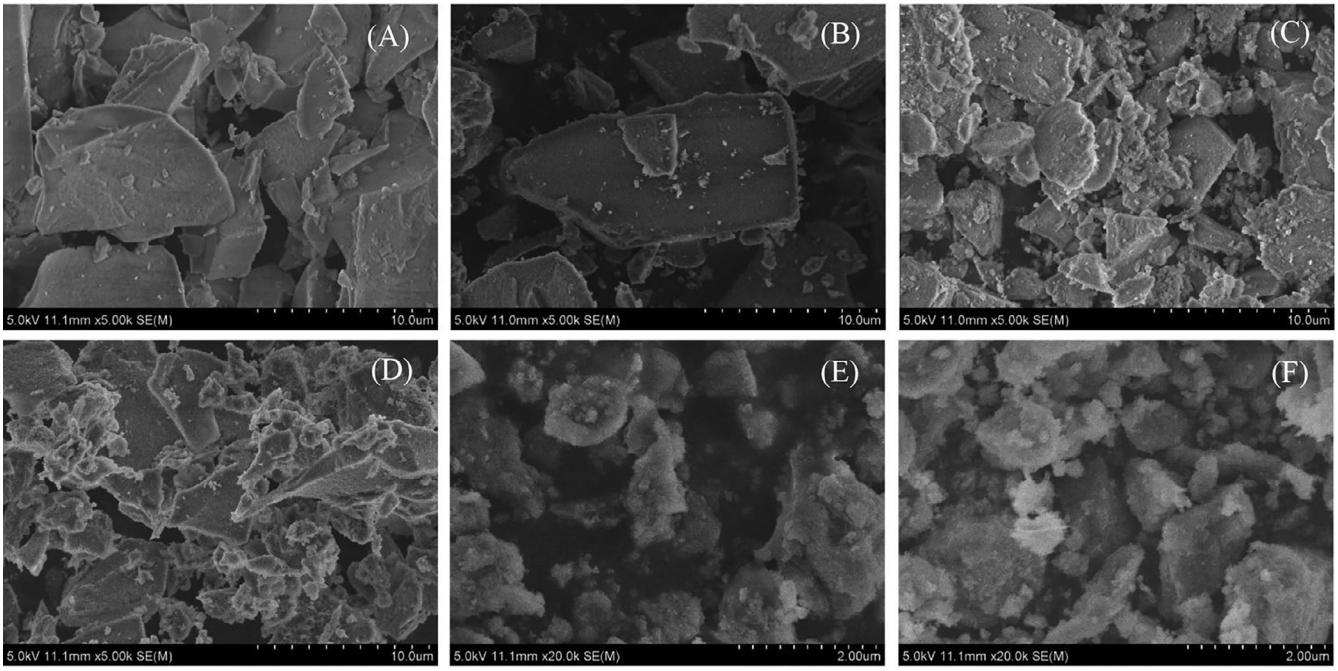

FIGURE 3 High resolution-scanning electron microscopy images of 5% Ag/γ-Al_2O_3 catalysts prepared at various hydrolysis pH using single-step sol–gel method: (A) pH = 4.0, (B) pH = 4.7, (C) pH = 5.0, (D) pH = 5.5, (E) pH = 5.7, and (F) pH = 6.0.

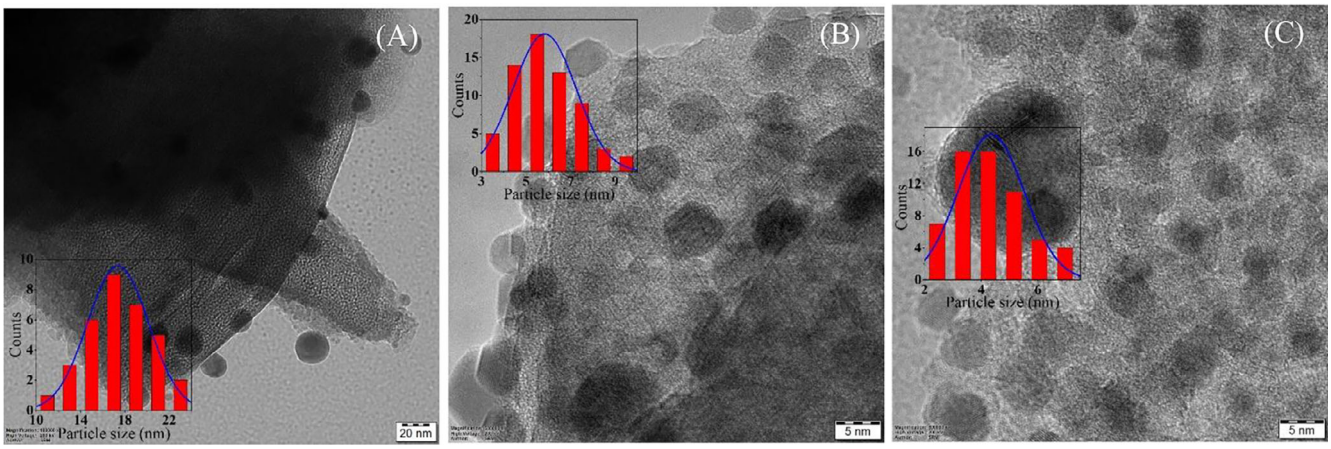

FIGURE 4 High resolution-scanning electron microscopy images of 5%Ag/γ-Al_2O_3 prepared by SSG method at various hydrolysis pH: (A) 4.0, (B) 5.0, and (C) 5.7. The inset shows the particle size distribution.

particles with parallel orientation.[43] The formation of a poorly connected network of boehmite particles is clearly evidenced by both the XRD and HR-SEM results at lower pH values. At higher pH levels, controlled hydrolysis-condensation processes yield well-crystallized smaller particles. The EDX analysis of the samples reveals the presence of the constituent elements and also that the estimated Ag-loading on the γ-Al_2O_3 support is 5 wt.% with ±0.5 wt.% deviation.

Figure 4 illustrates the HR-TEM images of various Ag/γ-Al_2O_3 catalysts. These micrographs show that the influence of pH on the variation of silver nanoparticles size and dispersion on the alumina support is strong. Furthermore, the Ag/γ-Al_2O_3 catalyst, which is synthesized at lower pH = 4.0, shows larger size silver nanoparticles with an average size of 17 nm, whereas the catalysts prepared at higher pH >5.0, indicates smaller silver nanoparticles with an average size of 7 nm at pH = 5.0 and 4 nm at pH = 5.7. On the other hand, at lower pH, there is improper dispersion of Ag nanoparticles over the γ-Al_2O_3 support, whereas, with an increase in pH, a remarkable improvement in the dispersion of nanoparticles is achieved. This will be of advantage in terms of catalytic activity as the activity for NOx

conversion can significantly be improved with a decrease in the size of the silver nanoparticles,[44,45] and improved dispersion. Thus, Ag/γ-Al_2O_3 catalysts prepared at higher pH result in high surface area and smaller silver nanoclusters with good dispersion on the support, which are presumably responsible for the enhanced activity of Ag-based catalysts, particularly at low temperatures. We hypothesize that this increase in activity with pH may be because of the varying ionic strength of the synthesis medium. The ionic strength in the medium influences the nanoparticle nucleation and growth and particle agglomeration.[46] Since pH is varied by adding different amounts of HNO_3, the ionic strength changes, resulting in changes in the morphological properties of the catalyst, as evidenced in the SEM and TEM micrographs as well (Figures 3 and 4).

3.1.4 | Preliminary catalyst evaluation studies

Before discussing the effect of pH on sol–gel synthesis, we first compare the catalyst prepared by SSG with that using the wet impregnation method in Figure 5. Specifically, as a part of optimizing the synthesis conditions for Ag/γ-Al_2O_3(SSG) catalysts, we tested the activities of the Ag/γ-Al_2O_3 catalysts prepared using the impregnation method over the sol–gel synthesized γ-Al_2O_3 (i.e., Ag/γ-Al_2O_3(WI)) and over the commercial γ-Al_2O_3 support (i.e., Ag/γ-Al_2O_3(SASOL)). The results were compared with the catalyst activity of unsupported γ-Al_2O_3 (without Ag loading) as well. It is clearly seen in Figure 5 that the presence of silver significantly improves the NOx conversion at all temperatures. Further, the catalysts synthesized using SSG method (SSG) showed better activity than those synthesized using wet impregnation. Therefore, for further evaluation of the catalyst, we employ the catalysts synthesized using the SSG process as they are expected to give highly reproducible and reliable results.

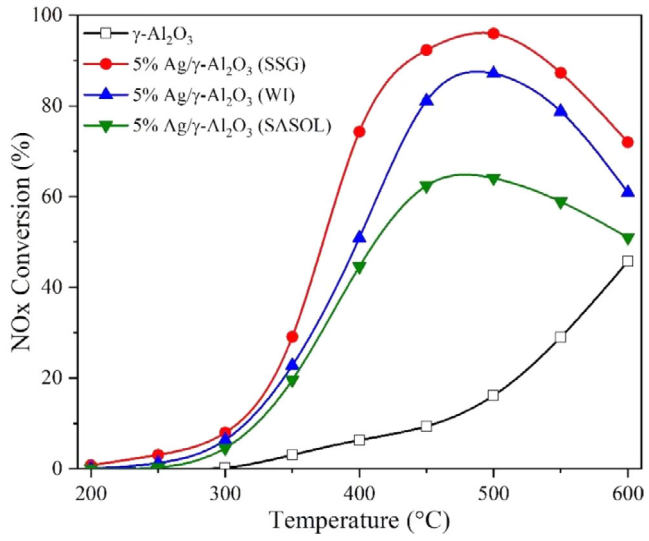

FIGURE 5 The catalytic activity results of 5%Ag/γ-Al_2O_3 catalysts prepared by different methods. Reaction conditions: 1.0 g catalyst, 980 ppm NO, 1050 ppm C_3H_6, 7 vol.% O_2 with a total flow rate of 600 mL min^{-1}. SSG, single-step sol–gel; WI, wet-impregnation.

3.2 | Catalyst performance

The variations in the catalytic activity for NOx reduction among catalysts prepared at different pH conditions of the synthesis medium yielded attractive results and are discussed in this section. The various characterization techniques indicated the role of synthesis conditions on the structural, textural, and morphological features of the catalysts.

3.2.1 | Role of pH on catalyst performance

Figure 6 shows the NOx conversion for the catalysts prepared at various hydrolysis pH. The activity of all the catalysts was tested using propylene (C_3H_6) as the reductant in excess oxygen in the temperature range 200–600°C with

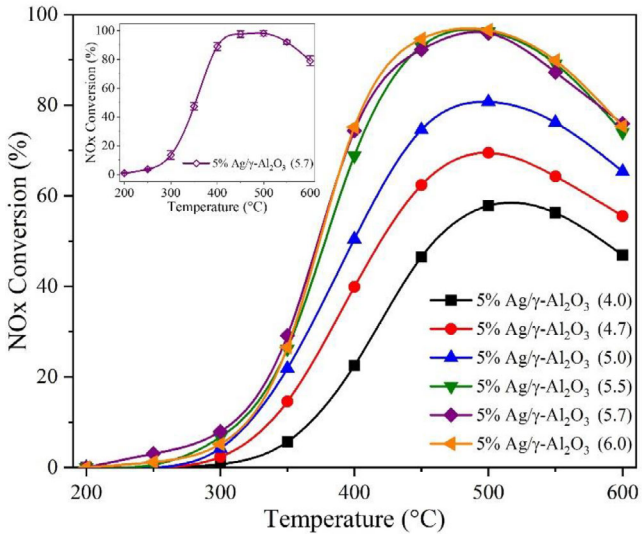

FIGURE 6 De-NOx activity for 5%Ag/γ-Al_2O_3 prepared at different pH. The numbers in the parentheses indicate the pH values of the synthesis medium. Reaction conditions: 1.0 g catalyst, 980 ppm NO, 1050 ppm C_3H_6, 7 vol.% O_2 with a total flow rate of 600 mL min^{-1}. The inset shows the reproducibility results of three batches of 5%Ag/γ-Al_2O_3 catalyst prepared at pH = 5.7. Reaction conditions: 1.0 g catalyst, 780 ppm NO, 1170 ppm C_3H_6, 7 vol.% O_2 with a total flow rate of 600 mL min^{-1}.

feed conditions of 980 ppm of NO, 1050 ppm of C_3H_6, 7 vol.% of O_2 and N_2 balance. The total flow rate into the reactor is 600 mL min^{-1}, and 1.0 g of catalyst is loaded into the reactor. It can be seen from Figure 6 that the Ag/γ-Al_2O_3 catalysts prepared at lower pH demonstrate lower catalytic activity, whereas catalysts prepared at higher pH demonstrate higher (> 90%) NOx conversion. Moreover, the peak temperatures (where conversion is maximum) shift to lower temperatures from 500 to 450°C. Further, a broader temperature activity window is observed with NOx conversion exceeding 70% over a temperature range from 400 to 600°C. The increase in NOx conversions for the catalysts prepared at higher pH (>5.0) can be attributed to the increase in surface area (cf. Table 1).

The synthesis procedure and reactor experiments are well reproducible for all the Ag loadings studied. The experiments were repeated at least three times each, and only minimal differences in NOx conversions were observed. The reproducibility of the activity of 5% Ag is highlighted and shown in Figure 6 (inset) as an example. The reproducibility was tested with the three different batches of the 5%Ag/γ-Al_2O_3 (5.7) catalyst, which was synthesized at the same hydrolysis pH = 5.7. The results indicate that the activity is highly reproducible demonstrating that the catalyst preparation method is reliable.

The effect of silver loading for NOx reduction has been studied extensively in the literature. Generally, lower Ag wt.% of 1–3%[4,27,47,48] give high conversions; however, they present narrow temperature activity windows. On the other hand, higher amount of Ag (>6 wt.%) yields lower deNOx activities[4,49] at higher temperatures. Overall, 4–6 wt.% catalysts tend to have the best combination of NOx conversion and broad temperature window.[4,27,32,33] This was evident in our experiments as well. The catalytic activity of the 5%Ag/γ-Al_2O_3 (5.7) was tested and compared with the catalytic activities of different Ag loaded, that is, 3%Ag/γ-Al_2O_3(5.7) and 7%Ag/γ-Al_2O_3 (5.7) catalysts. All the catalysts showed high NOx conversions. Although 3%Ag/γ-Al_2O_3 (5.7) showed higher NOx conversion at high temperatures, it was not active below 350°C, whereas 7%Ag/γ-Al_2O_3 (5.7) catalyst exhibited a decrease in activity at higher temperatures. Overall, 5%Ag/γ-Al_2O_3 (5.7) catalyst showed better catalytic performance over a broad temperature range (results are not shown here for the sake of brevity).

3.3 | Effect of operating conditions

3.3.1 | Time-on-stream studies

The time-on-stream studies were performed continuously with the 5%Ag/γ-Al_2O_3 (5.7) catalyst in the packed-bed reactor at 400°C for 50 h of time. The catalyst temperature was increased with a ramp rate of 2°C/min under N_2 flow, as before, and held at this temperature for an hour. Thereafter, the reactor feed was switched as follows: 970 ppm of NO, 1170 ppm of C_3H_6, and 7 vol.% O_2 with the 1.0 g catalyst loading at a total flow rate of 600 mL min^{-1}. The NOx conversions were consistently over 80%, and the catalyst was stable over the entire period of time without any observable loss in activity.

3.3.2 | Effect of feed ratio

Figure 7 illustrates the catalytic activity tests performed at different nitric oxide and propylene inlet concentrations; with an increase in the C_3H_6:NO ratio, there is an increase in NOx conversion. This was especially significant at lower temperatures. At C_3H_6:NO = 2.25, the optimized catalyst showed >50% NOx conversion even at 300°C. This light-off temperature is lower than previously reported in the literature. This may be attributed to the activation of propylene and the formation of oxygenates ($C_xH_yO_z$) in the low-temperature range over the smaller-sized Ag clusters. Moreover, the catalyst showed a broad activity temperature window in the temperature range of 320–600°C with more than 70% NOx conversion.

Figure 8 shows significant improvements in NOx conversions: From 8% to 55% at 300°C, from 26% to 85% at 350°C, and from 65% to 99% at 400°C, with increased propylene concentrations from the C_3H_6:NO ratio of 0.9 to 2.2. This increase in NOx conversions at higher

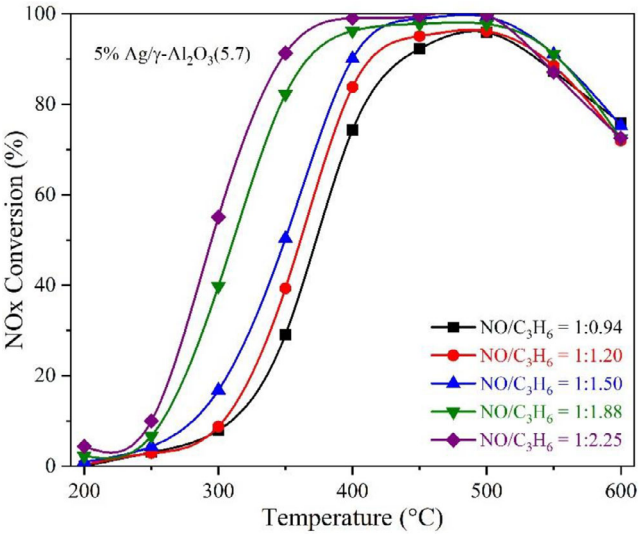

FIGURE 7 Catalytic activities of 5% Ag/γ-Al_2O_3 (5.7) catalyst at different ratios of NO and C_3H_6. Reaction conditions: 1.0 g catalyst, different ratios of NO to C_3H_6 at constant 7 vol.% O_2 with a total flow rate of 600 mL min^{-1}.

C_3H_6:NO ratios is due to the availability of propene for NOx reduction. The limits of C_3H_6 to NO ratios were chosen to be representative of typical automotive exhaust conditions, and not increased further though the results were promising. In summary, the synthesized catalysts at higher pH show higher activity for the entire temperature range, including light-off at relatively lower temperatures and higher propylene concentration.

3.3.3 | Effect of oxygen concentration

Figure 9 projects the effect of inlet O_2 concentration, from 3.4 to 12 vol.%, on the NOx conversion, keeping the NO:C_3H_6 ratio of 1:1.9. The catalyst performance for NOx reduction is similar for all conditions, as shown in Figure 9. Even at higher oxygen concentrations, the catalytic activity has no significant drop. The NOx conversions remain high, with a broad activity temperature window. There are slight differences in NOx conversions at higher temperatures beyond 500°C, for different inlet O_2 conditions, which may be attributed to a higher rate of propylene reaction with oxygen. But overall, the catalytic activities remained high even at higher temperatures with higher NOx conversions in excess oxygen concentrations.

3.3.4 | Effect of GHSV

The gas hourly space velocity (GHSV) is defined as the ratio of the volumetric flow rate to the active volume of the catalyst bed and was varied by varying the volumetric flow rate and catalyst loading. The catalytic activities were studied at GHSV of 30,000 to 120,000 h^{-1}. Catalysts were tested at different flow rates, namely, 600-, 900-, and 2400 mL min^{-1} at two different volumes of the catalyst—1.2 mL (which corresponds to 1.0 g of the catalyst) and 0.6 mL (0.5 g of the catalyst). We investigated catalyst activity at 30,000 h^{-1} (1.2 mL catalyst and 600 mL min^{-1} flow) as well as a high space velocity of 120,000 h^{-1} at (1.2 mL catalyst and 2400 mL min^{-1} flow). Figure 10 depicts the typical profile for different

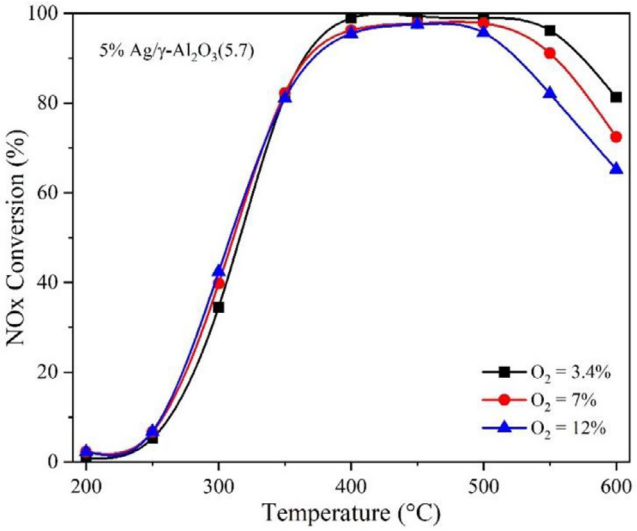

FIGURE 9 Catalytic activity of 5%Ag/γ-Al_2O_3 (5.7) catalyst at different concentrations of oxygen. Reaction conditions: 1.0 g catalyst, 520 ppm NO, 980 ppm C_3H_6, 3.4 vol.%, 7 vol.%, and 12 vol.% of O_2 with a total flow rate of 600 mL min^{-1}.

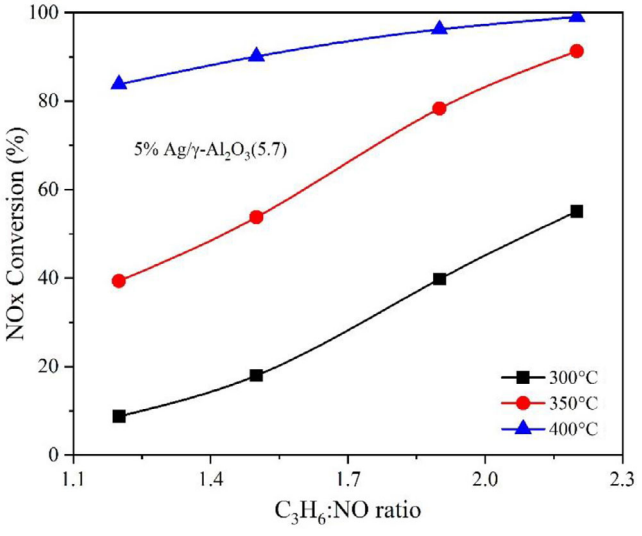

FIGURE 8 Catalytic activities of 5% Ag/γ-Al_2O_3 (5.7) catalyst at different ratios of NO and C_3H_6 at different temperatures. Reaction conditions: 1.0 g catalyst, 7 vol.% O_2, and flow rate of 600 mL min^{-1}.

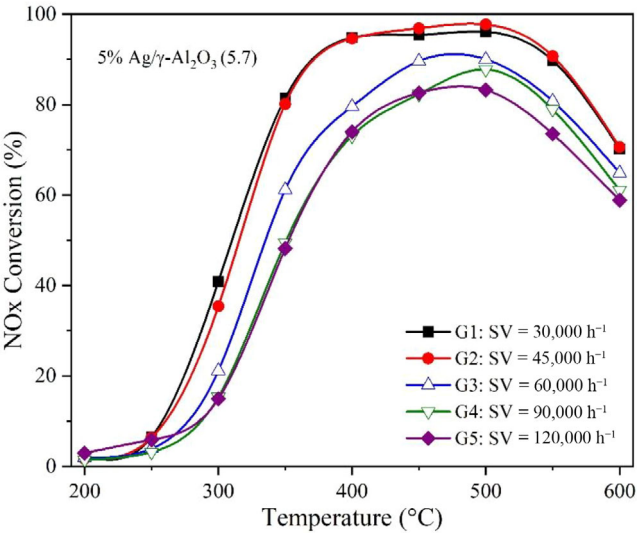

FIGURE 10 Catalytic activities of 5% Ag/γ-Al_2O_3 (5.7) catalyst at different space velocities. Reaction conditions: 520 ppm NO, 980 ppm C_3H_6, and 7 vol.% of O_2. SV, space velocity.

GHSV values. It can be seen from this figure that the NOx conversion is almost the same at GHSV values of 30,000 and 45,000 h^{-1} with a higher NOx conversion of 98% and NOx conversion exceeding 70% in the temperature range of 350–600°C. In other words, with the same catalyst loading (1.0 g; 1.2 mL), no drop in the activity was observed when the total flow rate was increased from 600 mL min^{-1} to 900 mL min^{-1}.

Likewise, the catalytic activity was also tested at higher space velocities, that is, at 60,000 h^{-1} and 90,000 h^{-1}. As shown in Figure 10, the NOx conversions were high with a broad activity temperature window. With a further decrease in the volume of the catalyst from 1.2 to 0.6 mL, that is, by reducing the loading of the catalyst from 1.0 to 0.5 g, there is only a slight drop in the NOx conversion. Finally, the catalytic activity test was done at very high space velocity, namely, at 120,000 h^{-1}, with a bed volume of 1.2 mL (1.0 g) by increasing the total flow rate to 2400 mL min^{-1}. Even at such a high space velocity, the catalyst performed exceptionally well. These results proved that even at higher space velocities and in excess amounts of oxygen, which are reasonably near-real diesel exhaust conditions, the optimized Ag/γ-Al_2O_3 catalysts could achieve excellent NOx conversions with the wider activity temperature window.

4 | KINETIC MODELLING AND REACTOR LEVEL SIMULATIONS

A generalized kinetic model is proposed to predict the activity of these catalysts in this section. In recent work,[50] a structure-dependent reduced global kinetic model is proposed and validated for SCR of NO with HCs for the Ag and Co catalytic systems. In particular, the effects of metal loading on catalyst performance are closely examined.[50] In this work, we developed a kinetic model to predict the activity of the catalysts described above, which are prepared at various hydrolysis pH. The kinetic model developed is based on the reaction scheme proposed by Azis et al.[51] for the SCR of Ag/γ-Al_2O_3 with a single surface site S1. The mechanism consists of five reactions: NO oxidation, propene oxidation, NO_2-assisted propene oxidation, selective reduction of NO by propene, and formation of surface nitrate, as listed in Table 2.[51] NO oxidation and surface nitrate formation are considered reversible reactions, and the latter is assumed to be in partial equilibrium. The equilibrium constant at any temperature T is given by the Vant Hoff's equation:

$$K_{eq}(T) = K_{298}\, e^{\frac{-\Delta H^{rxn}_{298}}{R}\left(\frac{1}{T}-\frac{1}{298}\right)}$$

Applying the partial equilibrium condition for R5 in the site conservation equation yields the site fractions θ_{S1} and θ_{S1-NO_3}. The equilibrium parameters (for R1 and R5) and rate constants are summarized in Table 2. While oxygen concentration was not considered for modelling the reaction system in Azis et al.,[51] in this work, oxygen is also considered in the reduction reaction (R4). Thus, the kinetic parameters of reactions R1, R2, R3, and R4, along with the order of reaction with respect to oxygen in reaction R4, are obtained by fitting the model to the experimental data. A pseudo-homogeneous plug flow reactor

TABLE 2 Reaction set is considered to model hydrocarbon-selective catalytic reduction (HC-SCR) and the corresponding rate constants.

Reactions		$\ln(k_0)$	$E_a\left(\frac{kJ}{mol}\right)$	K_{298}	$\Delta H^{rxn}_{298}\left(\frac{kJ}{mol}\right)$
R1	$NO + 0.5O_2 \overset{S1}{\leftrightarrow} NO_2$ $R_1 = k_1 y_{NO} y_{O_2}\left(1 - \frac{y_{NO_2}}{K_{eq_1} y_{NO} y_{O_2}}\right)\theta_{S1}$	5	21.0	15.6×10^5	−58.1
R2	$C_3H_6 + 4.5O_2 \overset{S1}{\rightarrow} 3CO_2 + 3H_2O$ $R_2 = k_2 y_{C_3H_6} y_{O_2} \theta_{S1}$	31.4*	189.0*		
R3	$9NO_2 + C_3H_6 \overset{S1}{\rightarrow} 3CO_2 + 9NO + 3H_2O$ $R_3 = k_3 y_{NO_2} y_{C_3H_6} \theta_{S1}$	33	57.8		
R4	$C_3H_6 + NO + 4O_2 \overset{S1}{\rightarrow} 0.5N_2 + 3CO_2 + 3H_2O$ $R_4 = k_4 y_{C_3H_6} y_{NO} y^n_{O_2} \theta_{s1}$	25.37*	87.1*		
R5	$NO + O_2 + S1 \leftrightarrow S1 - NO_3$ $\theta_{S1-NO_3} = K_{eq_5} y_{NO} y_{O_2} \theta_{S1}$			7.8×10^5	−18.1

Note: S1 denotes the empty site. θ_{s1} and θ_{s1-NO_3} denote the fractional coverages of the empty site and surface nitrate species. Reaction R5 is in partial equilibrium. The quantities marked with an asterisk (*) in the table can be varied as $(17.36 + 2.4\alpha)$, $(102.3 + 14.8\alpha)$ for R2 and $(21.47 + 0.7\alpha)$, $(105.47 - 3.18\alpha)$ for R4 to obtain to the kinetic parameters (k_0 & E_a) of the reaction system at other pH, where α represents pH of nitric acid used. The units of k_0 are such that the rate is in mol, kg, s.

model is solved by considering 1.0 g of catalyst to predict the outlet NOx conversion from the reactor. The kinetic parameters are obtained by fitting the kinetic model to the outlet NOx conversions at various temperatures shown in Figure 6, for the conditions: 980 ppm NO, 1050 ppm C_3H_6, and 7 vol.% O_2 with the flow rate of 600 mL min^{-1}.

Figure 11 depicts the conversion obtained by simulating the reactor with the kinetic model presented in Table 2 for the catalysts synthesized at a pH of 5.7. The non-monotonic variation in the NOx conversions versus reactor temperature is well predicted in the model simulations. At low temperatures, the surface nitrate formation is higher, and direct NO oxidation is low on Ag/γ-Al_2O_3 catalysts.[36,51,52] The surface coverage of nitrate species at 200°C is 0.8 and reduces to 0.12 at 600°C as predicted from the model, which is in agreement with earlier literature findings.[51,53] When most of the propene is utilized, such as at intermediate temperatures in the reactor, the conversion of NOx demonstrates a maximum. At higher temperatures, NOx conversion drops since propene is completely oxidized by oxygen preferentially. This can be confirmed by the rise in CO_2 (and H_2O) concentrations at higher temperatures. Consequently, unconverted NOx increases in the reactor at high temperatures. Overall, the proposed set of reactions, global rate expressions, and kinetic parameters reasonably predict the experimental data on NOx conversion in the catalytic reduction of NOx on Ag/γ-Al_2O_3 catalysts and capture the effect of catalyst synthesis conditions on the performance at the reactor level within the reaction conditions of interest.

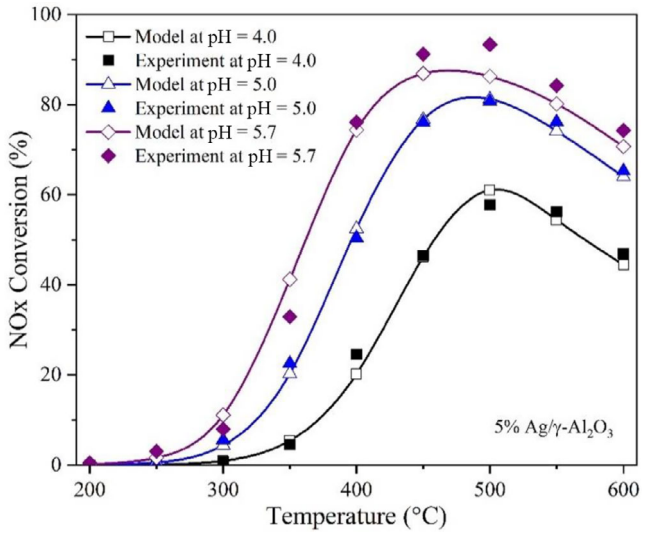

FIGURE 11 NOx conversion at various temperatures at pH = 5.7 (diamond) and feed conditions obtained from experiments (filled symbols), and model predictions (open symbols). NOx conversion at various temperatures at pH = 5.0 (triangle) and pH = 4.0 (square) at feed conditions. Model predictions are obtained from packed bed reactor simulations incorporating the kinetic model described in Table 2.

From the experimental results of Figure 6, we could also deduce that the catalysts prepared at various pHs follow the same trend in the conversion of NOx. However, the temperatures at which these catalysts activate, peak conversions, and temperature windows are significantly different. Therefore, it is supposed that the reactions (R1–R5) activate and proceed at different rates on catalysts prepared at various pH. A sensitivity analysis is performed at various temperatures (results not shown here for the sake of brevity), and it is observed that the reduction of NOx (R4) and complete oxidation of propene (R2) are the main reactions that determine the trend of the conversion of NOx. The direct oxidation of NO (R1) is difficult on Ag/γ-Al_2O_3, and the contribution of R3 is expected to be low owing to negligible NO_2 formed on the surface.[51,53,54] The kinetic model reported in Table 2 thus provides the values of the various fitted kinetic parameters—where the parameters for R2 and R4 are different at different synthesis conditions. A mathematical correlation is proposed to enable the prediction of NOx conversions of catalysts prepared at various pH. Figure 11 shows these predictions for the five reactions model of Table 2, with kinetic parameters of R4 and R2 varied for various pH, according to the correlation given in the table. It can be observed that the proposed kinetic model sufficiently predicts the various trends in NOx conversions.

The activity of supported metal catalysts is usually related to the amount of active phase dispersed.[55] However, in their studies, Arve et al.[44] could not relate the difference in the activity at different silver loadings to the dispersion and particle size alone. We believe that the differences in the catalytic activity in catalysts synthesized at various pH can really only be attributed to changes in kinetics—which manifests in different activation energies and other kinetic parameters in models. On a structural level, the differences may be ascribed to the existence of silver in various states on the support, which depends on the preparation method and the synthesizing conditions. The presence of silver in metallic, oxidized, and cluster forms was reported by many researchers.[15,24,36,44,54,56,57] Silver cations and oxidized silver clusters were reported in the presence of oxygen in the feed.[15,56] The effect of nitric acid leaching to remove weakly bound silver atoms was studied, where ionic silver bound to alumina was observed.[56] Ag^+ cations or oxidized silver clusters are known to favour the selective reduction of NO to N_2, whereas the metallic form of silver is known to favour the complete oxidation of HC[24,58] in other words, the

relative proportion of these forms of silver on the support may well determine overall activity. The HR-TEM image of our prepared catalyst (Figure 4) shows the presence of smaller nanoclusters. Therefore, the kinetic parameters, including activation energies, vary for catalysts prepared at various pHs, possibly due to the difference in the type of active site. At this time, we conclude our work with this statement. The kinetic model shown in Table 2 is a structure-sensitive one, which specifically, through fitting to lab-scale experiments, presents the kinetic parameters of relevance for NOx-SCR on sol–gel Ag catalysts at a host of synthesis conditions. A more intimate and direct relationship between the structure of the catalyst, the kinetic model, and, therefore, the predicted reactor level performance may be explored in the future.

5 | CONCLUSIONS

The synthesis procedure of a catalyst has a significant impact on the structure and morphology and hence affects its activity. Synthesis of 5%Ag/γ-Al_2O_3 catalysts was optimized for selective NOx reduction with propylene as a reducing agent (HC-SCR). The catalysts were synthesized using wet impregnation and SSG methods. Catalyst activity experiments for HC-SCR were performed in a packed-bed reactor with inlet feed of NO and C_3H_6 in the range of 500 to 2000 ppm in the presence of excess O_2. The catalysts prepared using the SSG method were more active toward HC-SCR.

The pH of the synthesis medium influences the nucleation and growth of nanoparticles and thus significantly impacts the morphological properties of the catalyst and its activity. At lower pH (<5.0), the catalyst was a mixture of phases, including an amorphous phase, which resulted in a lower surface area. A crystalline pseudo-boehmite structure was obtained at higher pH, which increased the surface area. The hydrolysis pH also affected the size of Ag nanoparticles and their dispersion over the alumina support.

A kinetic model that can predict the catalytic activity over the range of temperatures was developed. The kinetic analysis corroborated that those catalysts prepared by varying the hydrolysis pH resulted in different kinds of active sites, leading to differences in the activation energy and other kinetic parameters associated with the surface reactions.

Detailed analysis of morphology and activity of the optimized catalyst, combined with a kinetic model, demonstrated that high surface area and small size of well-dispersed Ag clusters enhance the activity toward NOx reduction. The optimized 5%Ag/γ-Al_2O_3 (pH = 5.7) catalyst showed the excellent time on stream behaviour (with no change in activity over a 50-hour period), a broad activity temperature window (of 300 to 600°C), and good activity at higher inlet oxygen conditions and higher space velocities as well. The effect of inlet conditions was analyzed: At higher propylene:NOx inlet ratio, the optimized catalyst showed higher activity and lower light-off temperature compared to prior reports in the literature.

AUTHOR CONTRIBUTIONS

Shivaraj Kumar Kummari: Conceptualization; investigation; methodology; writing – original draft. **Neha Yedala:** Investigation; software. **Parasuraman Selvam:** Conceptualization; supervision; writing – review and editing. **Niket S. Kaisare:** Conceptualization; supervision; writing – review and editing. **Preeti Aghalayam:** Conceptualization; funding acquisition; supervision; writing – original draft.

ACKNOWLEDGEMENTS

The authors thank for the financial support from the Ucchatar Avishkar Yojana (UAY)—Indian Science, Technology & Innovation Scheme, Chemical Engineering Department, IIT-Madras. The authors also thank the Department of Science & Technology (DST), New Delhi for supporting National Centre for Catalysis Research (NCCR), IIT-Madras.

CONFLICT OF INTEREST STATEMENT

There are no conflicts of interest to declare.

PEER REVIEW

The peer review history for this article is available at https://www.webofscience.com/api/gateway/wos/peer-review/10.1002/cjce.24967.

DATA AVAILABILITY STATEMENT

The data that support the findings of this study are available from the corresponding author upon reasonable request.

ORCID

Niket S. Kaisare https://orcid.org/0000-0001-9395-8784

REFERENCES

[1] T. Miyadera, *Appl. Catal., B* **1993**, *2*, 199.
[2] R. Burch, P. J. Millington, *Catal. Today* **1996**, *29*, 37.
[3] E. Seker, E. Gulari, *J. Catal.* **2000**, *194*, 4.
[4] E. Seker, J. Cavataio, E. Gulari, P. Lorpongpaiboon, S. Osuwan, *Appl. Catal., A* **1999**, *183*, 121.
[5] A. Kotsifa, T. I. Halkides, D. I. Kondarides, X. E. Verykios, *Catal. Lett.* **2002**, *79*, 113.
[6] K. Sato, T. Yoshinari, Y. Kintaichi, M. Haneda, H. Hamada, *Appl. Catal., B* **2003**, *44*, 67.

[7] A. Abu-Jrai, A. Tsolakis, *Int. J. Hydrogen Energy* **2007**, *32*, 2073.
[8] H. Dong, S. Shuai, R. Li, J. Wang, X. Shi, H. He, *Chem. Eng. J.* **2008**, *135*, 195.
[9] K. Theinnoi, S. Sitshebo, V. Houel, R. R. Rajaram, A. Tsolakis, *Energy Fuels* **2008**, *22*, 4109.
[10] S. Sitshebo, A. Tsolakis, K. Theinnoi, J. Rodríguez-Fernández, P. Leung, *Chem. Eng. J.* **2010**, *158*, 402.
[11] T. Miyadera, K. Yoshida, *Chem. Lett.* **1993**, *22*, 1483.
[12] T. N. Angelidis, N. Kruse, *Appl. Catal., B* **2001**, *34*, 201.
[13] Z. Li, M. Flytzani-stephanopoulos, *Appl. Catal., A* **1997**, *165*, 15.
[14] Z. Li, M. Flytzani-Stephanopoulos, *J. Catal.* **1999**, *182*, 313.
[15] T. Furusawa, K. Seshan, J. A. Lercher, L. Lefferts, K. I. Aika, *Appl. Catal., B* **2002**, *37*, 205.
[16] C. Shi, M. J. Cheng, Z. P. Qu, X. F. Yang, X. H. Bao, *Appl. Catal., B* **2002**, *36*, 173.
[17] R. Burch, S. Scire, *Appl. Catal., B* **1994**, *3*, 295.
[18] E. F. Iliopoulou, A. P. Evdou, A. A. Lemonidou, I. A. Vasalos, *Appl. Catal., A* **2004**, *274*, 179.
[19] R. Burch, T. C. Watling, *Appl. Catal., B* **1997**, *11*, 207.
[20] V. S. Prasad, P. Aghalayam, *Ind. Eng. Chem. Res.* **2016**, *55*, 9362.
[21] V. S. Prasad, P. Aghalayam, *Ind. Eng. Chem. Res.* **2017**, *56*, 11705.
[22] D. Bhatia, R. W. McCabe, M. P. Harold, V. Balakotaiah, *J. Catal.* **2009**, *266*, 106.
[23] R. Burch, P. J. Millington, *Catal. Today* **1995**, *26*, 185.
[24] K. A. Bethke, H. H. Kung, *J. Catal.* **1997**, *172*, 93.
[25] R. Burch, J. P. Breen, F. C. Meunier, *Appl. Catal., B* **2002**, *39*, 283.
[26] N. Hickey, P. Fornasiero, J. Kašpar, M. Graziani, G. Martra, S. Coluccia, S. Biella, L. Prati, M. Rossi, *J. Catal.* **2002**, *209*, 271.
[27] F. C. Meunier, R. Ukropec, C. Stapleton, J. R. H. Ross, *Appl. Catal., B* **2001**, *30*, 163.
[28] S. Satokawa, J. Shibata, K.-I. Shimizu, A. Satsuma, T. Hattori, *Appl. Catal., B* **2003**, *42*, 179.
[29] A. Martinez-Arias, M. Fernández-Garcıa, A. Iglesias-Juez, J. A. Anderson, J. C. Conesa, J. Soria, *Appl. Catal., B* **2000**, *28*, 29.
[30] R. Brosius, K. Arve, M. H. Groothaert, J. A. Martens, *J. Catal.* **2005**, *231*, 344.
[31] N. N. González Hernández, J. L. Contreras, M. Pinto, B. Zeifert, J. L. Flores Moreno, G. A. Fuentes, M. E. Hernández-Terán, T. Vázquez, J. Salmones, J. M. Jurado, *Catalysts* **2020**, *10*, 1.
[32] H. He, Y. Yu, *Catal. Today* **2005**, *100*, 37.
[33] G. Xu, J. Ma, G. He, Y. Yu, H. He, *Appl. Catal., B* **2017**, *207*, 60.
[34] F. Gunnarsson, H. Kannisto, M. Skoglundh, H. Härelind, *Appl. Catal., B* **2014**, *152–153*, 218.
[35] A. Keshavaraja, X. She, M. Flytzani-Stephanopoulos, *Appl. Catal., B* **2000**, *27*, L1.
[36] K.-I. Shimizu, J. Shibata, H. Yoshida, A. Satsuma, T. Hattori, *Appl. Catal., B* **2001**, *30*, 151.
[37] X. Du, Y. Wang, X. Su, J. Li, *Powder Technol.* **2009**, *192*, 40.
[38] B. E. Yoldas, *J. Appl. Chem. Biotechnol.* **2007**, *23*, 803.
[39] Y. Yang, Y. Xu, B. Han, B. Xu, X. Liu, Z. Yan, *J. Colloid Interface Sci.* **2016**, *469*, 1.
[40] S. Brunauer, L. S. Deming, E. Deming, E. Teller, *J. Am. Chem. Soc.* **1940**, *62*, 1723.
[41] K. S. W. Sing, R. T. Williams, *Adsorpt. Sci. Technol.* **2004**, *22*, 773.
[42] R. Bardestani, G. S. Patience, S. Kaliaguine, *Can. J. Chem. Eng.* **2019**, *97*, 2781.
[43] K. C. Song, I. J. Chung, *J. Non-Cryst. Solids* **1989**, *108*, 37.
[44] K. Arve, K. Svennerberg, F. Klingstedt, K. Eränen, L. R. Wallenberg, J. O. Bovin, L. Čapek, D. Y. Murzin, *J. Phys. Chem. B* **2006**, *110*, 420.
[45] H. Deng, Y. Yu, F. Liu, J. Ma, Y. Zhang, H. He, *ACS Catal.* **2014**, *4*, 2776.
[46] L. Al-Gebory, M. P. Mengüç, *J. Quant. Spectrosc. Radiat. Transfer* **2018**, *219*, 46.
[47] T. Chaieb, L. Delannoy, C. Louis, C. Thomas, *Appl. Catal., B* **2013**, *142–143*, 780.
[48] T. Chaieb, L. Delannoy, G. Costentin, C. Louis, S. Casale, R. L. Chantry, Z. Y. Li, C. Thomas, *Appl. Catal., B* **2014**, *156–157*, 192.
[49] H. Kannisto, K. Arve, T. Pingel, A. Hellman, H. Härelind, K. Eränen, E. Olsson, M. Skoglundh, D. Y. Murzin, *Catal. Sci. Technol.* **2013**, *3*, 644.
[50] N. Yedala, P. Aghalayam, *Chem. Eng. Res. Des.* **2022**, *181*, 110.
[51] M. M. Azis, H. Härelind, D. Creaser, *Chem. Eng. J.* **2015**, *278*, 394.
[52] S. Kameoka, Y. Ukisu, T. Mryadera, *Phys. Chem. Chem. Phys.* **2002**, *2*, 367.
[53] D. Creaser, H. Kannisto, J. Sjöblom, H. H. Ingelsten, *Appl. Catal., B* **2009**, *90*, 18.
[54] R. Lanza, E. Eriksson, L. J. Pettersson, *Catal. Today* **2009**, *147*, 279.
[55] F. C. Meunier, V. Zuzaniuk, J. P. Breen, M. Olsson, J. R. H. Ross, *Catal. Today* **2000**, *59*, 287.
[56] X. She, M. Flytzani-Stephanopoulos, *J. Catal.* **2006**, *237*, 79.
[57] A. Satsuma, K.-I. Shimizu, *Prog. Energy Combust. Sci.* **2002**, *29*, 71.
[58] N. Bogdanchikova, F. C. Meunier, M. Avalos-Borja, J. P. Breen, A. Pestryakov, *Appl. Catal., B* **2002**, *36*, 287.

How to cite this article: S. K. Kummari, N. Yedala, P. Selvam, N. S. Kaisare, P. Aghalayam, *Can. J. Chem. Eng.* **2023**, 1. https://doi.org/10.1002/cjce.24967